Optical properties of metal nanoparticles with no center of inversion symmetry: Observation of volume plasmons

Maxim Sukharev, Jiha Sung, Kenneth G. Spears, and Tamar Seideman
Department of Chemistry, Northwestern University, 2145 Sheridan Road, Evanston, Illinois 60208-3113, USA
(Received 4 August 2007; revised manuscript received 30 September 2007; published 13 November 2007)

We present theoretical and experimental studies of the optical response of L-shaped silver nanoparticles. The scattering spectrum exhibits several plasmon resonances that depend sensitively on the polarization of the incident electromagnetic field. The physical origin of the resonances is traced to different plasmon phenomena. In particular, a high energy band with unusual properties is interpreted in terms of volume plasmon oscillations arising from the asymmetry of a nanoparticle.

DOI: 10.1103/PhysRevB.76.184302 PACS number(s): 78.67.−n, 78.67.Bf, 78.70.−g, 78.20.Bh

I. INTRODUCTION

The fast progress in fabrication methods[1,2] of metallic nanoparticles (MNPs) and their arrays, along with the advances in laser technology,[2] has enabled a wide variety of applications of nanostructured materials in medicine,[3] biology,[4] chemistry,[5] and applied physics.[6] The recent literature suggests further potential applications of MNP arrays to guide light in the nanoscale and to study fundamental questions in wave propagation in confined space.[7] The optical properties of MNPs, and their sensitivity to the particle's shape, relative arrangement, and surrounding medium,[8] result from strong enhancement of an incident field at the plasmon resonance frequency,[9] where the light frequency matches the frequency of collective oscillations of the conduction electrons in the particle. MNPs with different shapes exhibit a variety of plasmon resonances ranging from dipole resonances in the quasistatic (diameter$\ll$wavelength) single sphere limit[10] to quadrupole and multipole modes in larger spheres,[11] nanocubes,[12] and other structures.[13] Particles of spheroidal shapes have also been a subject of intensive research,[14] showing multiple-peak scattering spectra.[15] Recently, it was suggested that MNPs without a center of inversion symmetry may be used for efficient second harmonic generation.[16]

The tremendous progress in the fabrication of MNPs and analysis of their properties notwithstanding, several fundamental aspects of plasmonics remain unclear. In particular, recent experiments on silver L-shaped nanoparticles and their arrays[17] raise questions on the physical origin of the multiband scattering spectrum and its dependence on the external field polarization. In this contribution, we present a systematic study of the optical response of a single L-shaped MNP and scrutinize the behavior of electromagnetic near fields at the resonant frequencies in order to explain the observed plasmon resonances and their physical nature. First, we discuss the theory and its numerical implementation. Next, we compare our simulations with experimental measurements. Finally, we discuss the physical content of each of the plasmon resonances of the L particle and introduce the volume plasmon mode as a possible interpretation of the high energy band observed in experiments.

II. THEORY

The interaction of metallic nanoparticles with electromagnetic (EM) radiation is simulated using a finite-difference time-domain[18] (FDTD) approach in three dimensions. The optical response of the metal is modeled using the auxiliary differential equation method[19] and the standard Drude model, within which the dielectric constant is given as

$$\varepsilon(\omega) = \varepsilon_\infty - \frac{\omega_p^2}{\omega^2 + i\Gamma\omega}, \tag{1}$$

where ε_∞ is the dimensionless infinite-frequency limit of the dielectric constant, ω_p is the bulk plasma frequency, and Γ is a damping constant. In order to simulate an open system, we implement perfectly matched layers (PMLs) absorbing boundaries with the exponentially differenced equations, so as to avoid diffusion instabilities.[20] As an incident light source, we use a linearly polarized plane wave, which is numerically generated at each point of a chosen xy plane placed above the metal particle and located near the upper PML region. In order to produce a pure plane wave and avoid the accumulation of spurious electric charges at the boundaries of the excitation plane, we embed its ends in PML regions. The parameters used in our simulations are provided in Ref. 21.

The optical response is simulated using a short-pulse excitation procedure described elsewhere.[22,23] First, we excite the particle by an ultrashort, linearly polarized pulse (the excitation pulse need be sufficiently short to span the range of frequencies of relevance; here, we used pulses of 0.36 fs duration). Next, we propagate the Maxwell equations in time for ~60 fs, recording the electric field components as functions of time at a fixed point in space. Finally, we perform a fast Fourier transformation to generate the spectra. The main advantage of this procedure is that one is able to recover the optical response of a given structure in terms of different electric field components. As shown below, it enables us to analyze quantitatively the behavior of the electric field induced by the asymmetric nanoparticles. Likewise informative are the vectorial eigenmodes of the system. The latter can be visualized using phasor functions,[18] which represent steady-state solutions of Maxwell's equations for cw excitation at the frequency corresponding to one of the eigenenergies of the particle,

$$\breve{E}_n(\vec{r};\omega) = \rho_n(\vec{r};\omega)\exp(i\phi_n(\vec{r};\omega)), \tag{2}$$

where $n=x,y,z$, and ρ_n and ϕ_n denote the amplitude and phase of the phasor, respectively. The phasors in Eq. (2) are

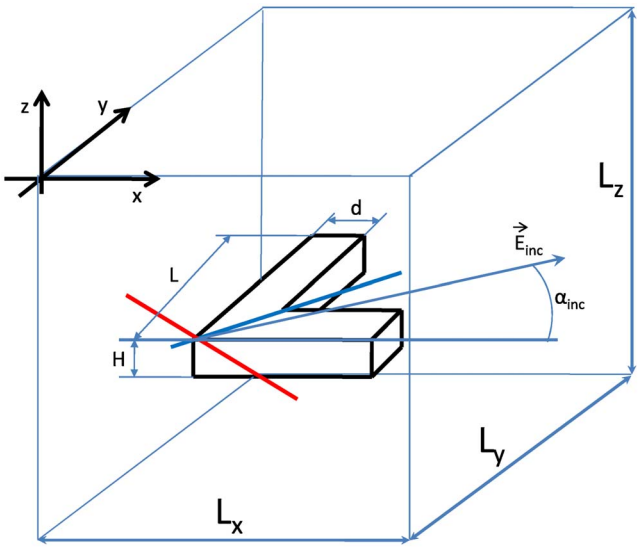

FIG. 1. (Color online) Schematic setup of the FDTD simulations. $L_{x,y,z}$ denotes the size of the simulation cube. L, d, and H represent the arm length, the thickness, and the height of the L particle respectively; here, $L=150$ nm, $d=60$ nm, and $H=30$ nm. The particle is excited by an EM plane wave that is generated five steps below the upper xy-PML region and is propagated along the z direction. The parameter α_{inc} defines the relative orientation of the particle with respect to the incident EM field. The red and blue lines represent the two axes of symmetry of the particle.

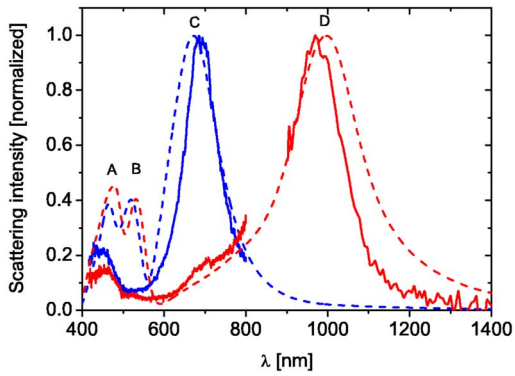

FIG. 2. (Color online) Normalized experimental (solid curves) and theoretical (dashed curves) scattering intensity as functions of the incident wavelength λ. The blue curves correspond to $\alpha_{inc}=\pi/4$ (the incident field polarization is along the blue axis of symmetry in Fig. 1). The red curves correspond to $\alpha_{inc}=3\pi/4$ (the incident field polarization is along the red axis of symmetry in Fig. 1). A, B, C, and D indicate the four resonances that are discussed in the text. Simulations are performed for a particle embedded in nondispersive media with refractive index $n_{eff}=1.3$. The small peak near 700 nm that can be seen at the shoulder of red band (solid red line) is due to polarization impurity in the dark-field scattering setup. This band was not observed with pure polarization in two-dimensional array extinction measurements (Ref. 17).

computed via a recursive discrete Fourier transform "on the fly" within a single FDTD run.[18] In order to obtain the correct phasor functions (i.e., their amplitudes and phases), one has to choose carefully the propagation time of electromagnetic field. In numerical experiments, we found that for a plane wave incident source with a time dependence of the $\sin(\omega t)$ form (ω corresponding to the one of eigenfrequencies of the structure), the calculation is numerically converged with 100 fs propagation time.

In this work, we consider the optical properties of L-shaped silver nanoparticles, as depicted schematically in Fig. 1. All simulations are performed on the BlueGene/L supercomputer at Argonne National Laboratories. In order to partition the FDTD scheme onto a parallel grid, we divide the simulation cube into 64 slices along the z axis, see Fig. 1, and implement point-to-point MPI communication subroutines at the boundaries between slices. The number of xy planes in each slice varies from 5 to 10. For an FDTD cube of size $L_x \times L_y \times L_z = 264 \times 264 \times 384$ nm^3 and a step size $\delta=1.2$ nm, a single run that propagates the EM fields for 60 fs takes on average ~80 min on 64 processors.

III. RESULTS AND DISCUSSION

We begin this section by comparing the FDTD simulations described in the previous section with measurements of scattering and extinction spectra of a single silver L particle for different polarizations of the incident field. Figure 2 presents both the experimental data and the numerical simulations. The latter involve ten independent FDTD runs, in which we calculated the scattering intensity along the incident field polarization for an L particle in vacuum, taking $\alpha_{inc}=\pi/4$ and $3\pi/4$ (see Fig. 1). The particle dimensions are $H=30$ nm, $L=145$ nm, and $d=60$ nm. In order to estimate the substrate effects, we introduce an effective refractive index n_{eff}. By comparing experimental and simulated resonant wavelengths for the blue ($\alpha_{inc}=\pi/4$) and red ($\alpha_{inc}=3\pi/4$) bands, we found that $n_{eff}=1.3$ best matches the experimental observations. Random deviations of the particle dimensions are accounted for by performing simulations for a small range of particle sizes and averaging the resulting spectra over the ensemble of different sized particle.

The experimental particles have random deviations in the particle arm length L and its thickness d. A previous publication[17] gives a detailed description of the sample fabrication and measurement setup. In brief, the two-dimensional square array of L-shaped silver nanoparticles was fabricated by electron-beam lithography on an indium tin oxide conducting layer of 40 nm on 750 μm thick glass substrate. The grid spacing of the nanoparticle array is 5 μm. The dipole interaction between particles is negligible at this grid spacing; therefore, each particle can be considered as an isolated particle. The particle arm length L, thickness d, and height H are 145 ± 8, 63 ± 4, and 30 nm, respectively. The tips of each nanoparticle are rounded, as seen in scanning electron microscope images (not shown). The blue band (C) and the high energy shoulder of the red band (D, 400–800 nm range) in Fig. 2 are dark-field scattering spectra of a selected nanoparticle within the sample with $\alpha_{inc}=\pi/4$ and $3\pi/4$, respectively. They are obtained on an inverted microscope equipped with a dark-field condenser and a spectrometer with a liquid nitrogen-cooled charge-coupled device detector.

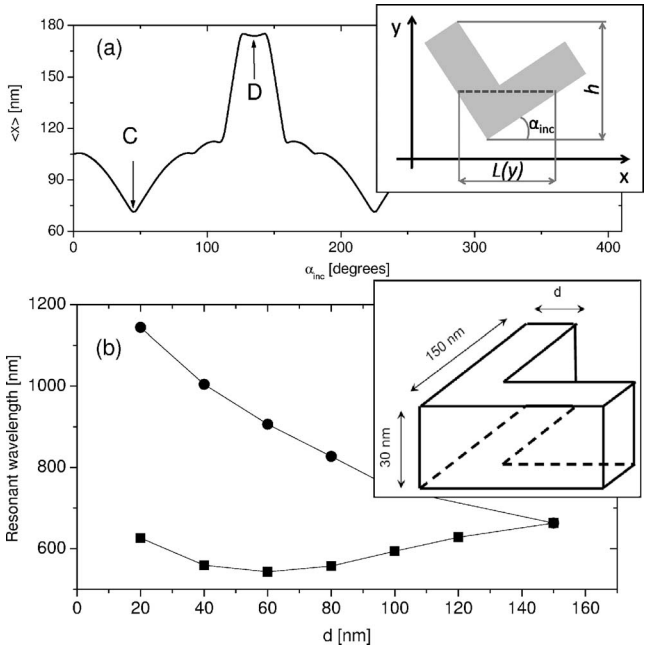

FIG. 3. (a) The concept of a shape functional—the average length of longitudinal plasmon oscillations, $\langle x \rangle$ (see the upper inset), as a function of the orientation of L box, α_{inc}. (b) The blue (squares) and red (circles) band positions (i.e., the C and D resonances in Fig. 2) vs the particle's arm thickness d. Simulations are performed for a particle embedded in a nondispersive media with refractive index $n_{\mathrm{eff}}=1.3$.

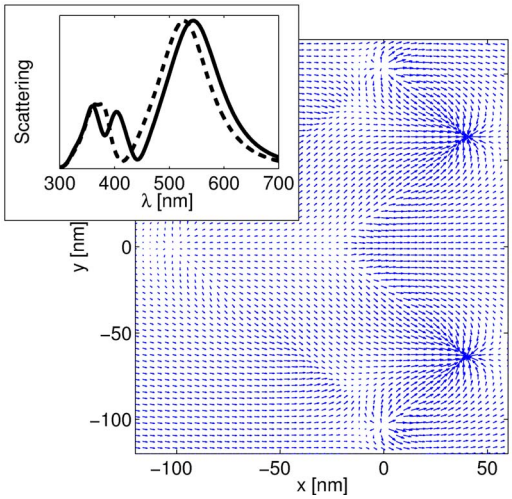

FIG. 4. (Color online) Inset: comparison of the scattered intensities as a function of the incident wavelength λ for L particles with sharp (solid curve) and with rounded (dashed curve) corners. The main panel shows the vector field xy distribution of electric field inside the particle for the B resonance (see Fig. 2). Simulations are performed for a particle in vacuum.

The red band (D, 900–1400 nm range) is the extinction spectrum of the sample with $\alpha_{\mathrm{inc}}=3\pi/4$, obtained with a laboratory-built microscope that records polarized extinction spectra over a spot diameter (full width at half maximum) of 20 μm.

Clearly, the optical response of the L particle is very sensitive to the incident field polarization and exhibits four resonant bands. We note that if the incident field polarization is not along one of two axes of symmetry ($\alpha_{\mathrm{inc}} \neq \pi/4, 3\pi/4$, see Fig. 1), the spectrum exhibits all the resonance features, with the amplitudes depending on α_{inc}. The physical origin of the blue (C) and red (D) bands can be understood through extension of the simple case of the eigenmodes of a simple metallic wire. Collective oscillations of conductive electrons along the wire axis leads to a low energy resonance, whereas oscillations perpendicular to the wire axis give rise to a higher energy band. For the case of a more complex structure, such as the L structure considered here, the concept of a shape functional[12,24] provides an analogous picture. The shape functionals determine the polarizability tensor of the particle and hence the response of the confined electrons to an external field. The inset of Fig. 3(a) describes schematically the construction of a shape functional. Consider an L-shaped two-dimensional box driven into oscillations along the x axis (corresponding to an L particle exposed to an x-polarized external electric field). The resonant wavelength of these oscillations is proportional to the average dimension

$$\langle x \rangle = \frac{1}{h} \int L(y) dy \tag{3}$$

and depends on the orientation of the particle with respect to the x axis [see the inset of Fig. 3(a)]. The dependence of $\langle x \rangle$ on the orientation, shown in the main panel of Fig. 3(a), exhibits two extrema, at $\alpha_{\mathrm{inc}}=\pi/4, 3\pi/4$. The two low energy bands become degenerate in the limit of a parallelepiped shape, as illustrated in the main panel of Fig. 3(b). Here, we show the resonant wavelengths of the C and D bands as functions of the thickness d of the L-particle arm starting from $d=20$ nm and ending with the parallelepiped case, $d=150$ nm. Whereas the energy of the red band (marked D) monotonically increases, that of the blue band (C) is nonmonotonic, shifting to the blue at small d and to the red subsequently. The latter corresponds to the case where the high energy bands A and B (see Fig. 2) strongly overlap with the blue band, resulting in broad spikes with a fine multipeak structure.

The origin of the resonance labeled B in Fig. 2 is the sharp corners of the L particle. It is well known that sharp features of metallic structures tend to accumulate surface charges and hence lead to strong EM field enhancements.[8] Figure 4 illustrates the vector field distribution of phasor functions (2), $\breve{E}_x(\vec{r};\omega)$ and $\breve{E}_y(\vec{r};\omega)$, in the xy plane at a distance of 3 nm above the particle at the wavelength of the resonance labeled B. It is seen that the corners enhance the EM field and that each corner gives rise to an oscillating dipole. In order to illustrate that the origin of the B resonance is the sharp corners, we perform simulations for an L-shaped particle with rounded corners. The inset of Fig. 4 compares the scattering intensity due to particles with sharp and with rounded corners, showing that for the latter the B resonance disappears. We note that a small blueshift of the blue band

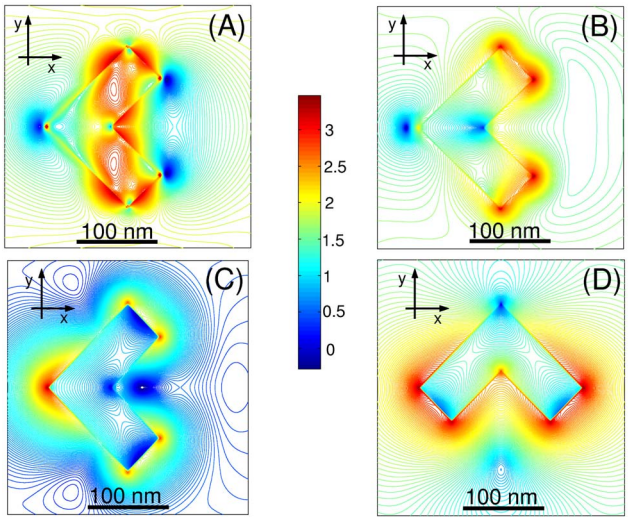

FIG. 5. (Color online) EM energy enhancement (the ratio of the total and incident energies) distributions of the plasmon eigenmodes in the L particle at $z=0$ (corresponding to the plane bisecting the particle) on a logarithmic scale. Panel (A) corresponds to the A resonance, panel (B) to the B resonance, panels (C) to the blue band, and panel (D) to the red band. The external EM field is polarized along the x axis with the propagation k vector perpendicular to the plane of the figure.

(C) for the particle with rounded corners is due to the fact that its volume in our simulations is slightly smaller than the volume of the L particle with sharp corners.

A particularly interesting result of this work is the observation of the high energy band, labeled A in Fig. 2. Its origin differs markedly from that of the features discussed above. Whereas the EM fields corresponding to resonances B, C, and D are mostly localized on the surface of the particle and can be readily explained in terms of surface plasmon modes, the EM field distributions in the case of the A resonance reveal complex volume oscillations. Figure 5 shows the xy distribution of EM energy calculated using the phasor function representation [Eq. (2)] at the middle of the particle for all four bands. It is evident that the EM energy is localized in the interior of the particle at the energy of band A. By contrast, similar plots at the energies of the remaining bands (not shown) emphasize the surface character of the response. Figure 5(a) also shows remarkably large fields inside the particle, reaching almost 3 orders of magnitude enhancements throughout the entire volume. Additional simulations, in which we varied the height of the particle, H, illustrate strong sensitivity of the A resonance to the volume of the particle, whereas the lower energy bands are essentially invariant to the volume. We also analyzed the density currents for all resonances and found that surface currents dominate the B, C, and D bands, whereas volume current in the particle plays a dominant role in the high energy band A. Although the behavior of the density currents at the energy of band A is similar to that of multipole oscillations, they differ qualitatively from the latter case in that (by contrast to the multipole modes[12]) they are not localized on the surface.

By numerically bending a metallic wire and calculating the scattering spectra as a function of the curvature of such arcuate particle, we verified that it is the breakdown of the inversion symmetry that gives rise to the volume plasmon modes, which are dipole forbidden for the symmetric particles. Another interesting observation of our simulations, which distinguishes the high energy band from the lower energy ones, is the number of oscillations per resonance lifetime, estimated as the ratio of the eigenenergy of the plasmon mode to its full width at half maximum.[25] We found that this ratio is about 3–4 for the C and D resonances, depending on the incident polarization, but noticeably larger (~ 8) for the volume plasmon band. It is interesting to note that a similar high energy band has been observed in recent experiments on crescent-shaped nanoparticles.[26]

IV. CONCLUSION

In the previous sections, we presented experimental measurements and numerical analysis of the optical properties of a single L-shaped silver nanoparticle. We showed that in addition to several resonances that are attributed to surface plasmon modes, L particles also support long-lived volume plasmon oscillations of conductive electrons, resulting in strong EM fields confined in the interior of the particle. Our numerical analysis suggests that volume plasmon modes can be found in spectra of other metallic nanoparticles without center of inversion symmetry. Among several extensions and applications of the present work, we plan to explore the optical response of arrays of asymmetric particles.

ACKNOWLEDGMENTS

This research was supported in part by the NCLT program of the National Science Foundation (ESI-0426328) at the Materials Research Institute of Northwestern University, and in part by the Air Force Office of Scientific Research (MURI program Grant No. F49620-02-1-0381). The numerical work used the resources of the Argonne Leadership Computing Facility at Argonne National Laboratory, which is supported by the Office of Science of the U.S. Department of Energy under Contract No. DE-AC02-06CH11357.

[1] E. Hutter and J. H. Fendler, Adv. Mater. (Weinheim, Ger.) **16**, 1685 (2004).
[2] R. E. Slusher, Rev. Mod. Phys. **71**, 00S471 (1999).
[3] A. H. Haes and R. P. Van Duyne, Expert Rev. Mol. Diagn. **4**, 527 (2004).
[4] P. Alivisatos, Nat. Biotechnol. **22**, 47 (2004).
[5] R. P. Van Duyne, Science **306**, 985 (2005).
[6] S. A. Maier and H. A. Atwater, J. Appl. Phys. **98**, 011101 (2005).
[7] M. Sukharev and T. Seideman, J. Phys. B **40**, S283 (2007).
[8] L. Novotny and B. Hecht, *Principles of Nano-Optics* (Cambridge

University Press, Cambridge, England, 2006).
[9] S. A. Maier, *Plasmonics: Fundamentals and Applications* (Springer, New York, 2007).
[10] U. Kreibig and M. Vollmer, *Optical Properties of Metal Clusters* (Springer, New York, 1995).
[11] A. S. Kumbhar, M. K. Kinnan, G. Chumanov, J. Am. Chem. Soc. **127**, 12444 (2005).
[12] R. Fuchs, Phys. Rev. B **11**, 1732 (1975).
[13] C. Noguez, J. Phys. Chem. C. **111**, 3806 (2007).
[14] H. C. van de Hulst, *Light Scattering by Small Particles* (Dover, New York, 1981).
[15] W. Gotschy, K. Vonmetz, A. Leitner, and F. R. Aussenegg, Opt. Lett. **21**, 1099 (1996).
[16] H. Tuovinen, M. Kauranen, K. Jefimovs, P. Vahimaa, T. Vallius, J. Turunen, N. V. Tkachenko, and H. Lemmetyinen, J. Nonlinear Opt. Phys. Mater. **11**, 421 (2002).
[17] J. Sung, E. M. Hicks, R. P. Van Duyne, and K. G. Spears, J. Phys. Chem. C. **111**, 10368 (2007).
[18] A. Taflove and S. C. Hagness, *Computational Electrodynamics: The Finite-Difference Time-Domain Method*, 3rd ed. (Artech House, Boston, 2005).
[19] R. M. Joseph, S. C. Hagness, and A. Taflove, Opt. Lett. **16**, 1412 (1991).
[20] M. N. O. Sadiku, *Numerical Techniques in Electromagnetics*, 2nd ed. (CRC, Boca Raton, FL, 2001).
[21] Drude parameters in Eq. (1) for silver used in our simulations are $\varepsilon_\infty = 8.926$, $\omega_p = 1.7601 \times 10^{16}$ rad/s, and $\Gamma = 3.0841 \times 10^{14}$ rad/s.
[22] S. K. Gray and T. Kupka, Phys. Rev. B **68**, 045415 (2003).
[23] M. Sukharev and T. Seideman, J. Chem. Phys. **126**, 204702 (2007).
[24] M. A. Karam, Appl. Opt. **36**, 5238 (1996).
[25] S. W. J. Scully, E. D. Emmons, M. F. Gharaibeh, R. A. Phaneuf, A. L. D. Kilcoyne, A. S. Schlachter, S. Schippers, A. Müller, H. S. Chakraborty, M. E. Madjet, and J. M. Rost, Phys. Rev. Lett. **94**, 065503 (2005).
[26] H. Rochholz, N. Bocchio, and M. Kreiter, New J. Phys. **9**, 53 (2007).